Transient Excitation of a Layered Dielectric Medium by a Pulsed Electric Dipole

Anton G. Tijhuis, *Member, IEEE*, and Amelia Rubio Bretones, *Senior Member, IEEE*

***Abstract*—In this paper, we consider the transient excitation by a pulsed vertical or horizontal dipole of a continuously layered lossy dielectric slab embedded in between two dielectric half-spaces. The focus of the paper is on finding a highly efficient numerical implementation. To this end, we choose all spatial approximations independent of frequency. In the first place, this concerns the inverse spatial Fourier transformation in the Sommerfeld representation of the fields. A suitable quadrature rule is obtained by introducing a normalized wave number, and identifying the result in terms of dual analytic signals. In the second place, this concerns the spectral fields for which a new integral equation is derived with a degenerate kernel. This integral equation is solved by a fully recursive procedure. Representative results are presented and discussed that can be underdstood from physical intuition.**

***Index Terms*—Dipole antennas, electromagnetic transient analysis, nonhomogeneous media, transient propagation.**

I. Introduction

AFTER almost 20 years, the first author still fondly remembers his first two encounters with Prof. James R. Wait. In the spring of 1981, Prof. Wait visited the Electromagnetics Laboratory, Delft University of Technology, The Netherlands. During that visit, he was kind enough to spend an afternoon with a young colleague who had just submitted his first two conference papers. Later that year, when these papers had to be presented at the URSI/AP-S meeting in Québec, Canada, he encountered the same young scientist in the shower room of the dormitories. Noticing the nervousness of the prospective speaker, Prof. Wait took the time to reassure him. Since then, there have been numerous encounters, which were always stimulating on a personal as well as on a scientific level.

Since both papers mentioned above dealt with transient fields in layered dielectric media, this will also be the topic of the present contribution. In particular, we deal with the efficient numerical computation of the transient field generated by a dipole source above a continuously layered slab in between two homogeneous half-spaces. From the many publications by Prof. Wait on this subject (see, e.g., [1] and [2]), we hope that this is a subject that he would have appreciated. The ideas presented in this paper have been available for several years and have already been used extensively for modeling the interaction between pulsed wire segments and loop antennas and stratified media [3]–[5]. The invitation to contribute to this special issue seemed like the perfect occasion to write a more fundamental paper about the basic formalism.

Obviously, when dealing with layered media, one uses spectral techniques. These techniques have been around for a long time; an excellent review of early work can, for example, be found in [6]. Expressions for the spectral fields in a piecewise homogeneous three-layer region were given in [7]. Only a few authors have devoted attention to the efficient evaluation of the spectral integrals. Possibly, this can be explained from the success of the fast Fourier transformation. Straightforward and advanced computations for half-spaces can, e.g., be found in [8] and [9].

Our approach is the spectral counterpart of the continuous-time discretized-space (CTDS) approach as explained for integral equations in [10] and [11]. The basic idea is that, under realistic restrictions on the transient behavior of the impressed current or incident field, all spatial approximations may be chosen independently of the frequency. The relative error in the frequency-domain spectral components will obviously increase with increasing frequency, but this does not affect the accuracy of the obtained time-domain results. At a first glance, this result seems counter-intuitive. However, even a well known technique like the FDTD essentially uses a fixed spatial approximation, followed by a time discretization. The only difference is that, in the CTDS approach, the time sampling is replaced by a frequency sampling, thus avoiding the error accumulation that is inherent in direct time-domain computations.

The key result in our approach is the normalization of the spatial wavenumber with respect to frequency. This idea is used in a slightly different manner in the Cagniard-De Hoop method. Classical applications of that method to piecewise homogeneous media can be found in [12], [13] and [14]. Approximate results for inhomogeneous media can be found in [15] and [16]. Our approach is different in the sense that we keep the frequency real, and allow the time variable to become complex. In this respect, our work also resembles the spectral theory of transients proposed in [17]–[20]. In addition to the spectral approach, we derive a new integral equation for the spectral fields, which, after a discretization that does not depend on the spectral parameters, can be solved recursively in $\mathcal{O}(M)$ operations for $M+1$ unknown field values.

The organization of the paper is quite straightforward. In Section II we formulate the problem, in Section III we consider the behavior of the spectral components, in Section IV the evaluation of the spectral integrals is addressed, and in Section V we

Manuscript received September 15, 1999. A. Rubio Bretones was supported by CICYT, Spain, under Project TIC98-1037-C03-01 and by the Philips Gift and the University Fund of the Eindhoven University of Technology.

A. G. Tijhuis is with the Telecommunication Technology and Electromagnetics Division, Faculty of Electrical Engineering, Eindhoven University of Technology, 5600 MB Eindhoven, The Netherlands (e-mail: a.g.tijhuis@tue.nl).

A. Rubio Bretones is with the Departamento de Electromagnetismo, Facultad de Ciencias, Universidad de Granada, 18071 Granada, Spain (e-mail: arubio@goliat.ugr.es).

Publisher Item Identifier S 0018-926X(00)09366-2.

present and discuss a few representative numerical results. Finally, some conclusions are formulated in Section VI.

II. Formulation of the Problem

We consider a configuration that consists of an isotropic, linearly and instantaneously reacting, horizontally stratified, lossy dielectric medium embedded between two homogeneous dielectric half-spaces $\mathcal{D}_1$ and $\mathcal{D}_3$ in $z < 0$ and $z > d$, respectively (Fig. 1). For convenience, the half-spaces are assumed to be lossless. However, the analysis presented in this paper can directly be generalized to the case of lossy half-spaces. The slab is located in the domain $\mathcal{D}_2$, with $0 < z < d$. The configuration is driven by a pulsed electric dipole whose current density is given by

$$\boldsymbol{\mathcal{J}}^i(\mathbf{r},t) = \partial_t \mathcal{S}(t)\delta(\mathbf{r} - z_0\mathbf{u}_z)\mathbf{u}_d \tag{1}$$

with $z_0 < 0$. In (1), the superscript i stands for "impressed". $\mathcal{S}(t)$ is a signal of finite duration and the time coordinate is chosen such that this pulse starts at $t = 0$. The time derivative has been included to ensure that the electric current does not leave behind a static charge distribution as $t \to \infty$. $\mathbf{u}_d$ is a unit vector. Because of the symmetry of the configuration, we may restrict ourselves to the cases where $\mathbf{u}_d = \mathbf{u}_z$ (vertical dipole) or $\mathbf{u}_d = \mathbf{u}_x$ (horizontal dipole).

The aim of the computation is to determine the transient electromagnetic field caused by the electric current distribution specified in (1). In particular, we are interested in the field in the upper half-space $z < 0$ since that is the field that can be detected by an antenna. Once this field is known, we can apply the superposition principle to determine the effect of a more general current distribution.

A. Transmission-Line Equations

Before we solve the specific problem formulated above, we first summarize the general transmission-line equations that govern the propagation of electromagnetic waves in a dielectric medium with permittivity $\varepsilon(z)$, conductivity $\sigma(z)$, and permeability $\mu(z)$. We follow the general formulation presented in [22], but we adapt the time dependence and the notation to the problem at hand. In the layered configuration specified above, the electromagnetic fields satisfy the following version of Maxwell's equations:

$$\nabla \times \boldsymbol{\mathcal{H}}(\mathbf{r},t) = [\varepsilon(z)\partial_t + \sigma(z)]\boldsymbol{\mathcal{E}}(\mathbf{r},t) + \boldsymbol{\mathcal{J}}^i(\mathbf{r},t) \tag{2a}$$

$$\nabla \times \boldsymbol{\mathcal{E}}(\mathbf{r},t) = -\mu(z)\partial_t \boldsymbol{\mathcal{H}}(\mathbf{r},t). \tag{2b}$$

To exploit the fact that the constitutive parameters in (2) depend only on the z-coordinate, we solve these equations in the spectral domain. To this end, we introduce the following temporal and spatial Fourier transformations:

$$\mathbf{E}(\mathbf{r},\omega) = \int_0^\infty \boldsymbol{\mathcal{E}}(\mathbf{r},t)\exp(i\omega t)\,dt \tag{3a}$$

$$\hat{\mathbf{E}}(\mathbf{k}_T,z,\omega) = \int_{-\infty}^{\infty}\int_{-\infty}^{\infty} \mathbf{E}(\mathbf{r},\omega)\exp(-i\mathbf{k}_T\cdot\mathbf{r}_T)\,dx\,dy \tag{3b}$$

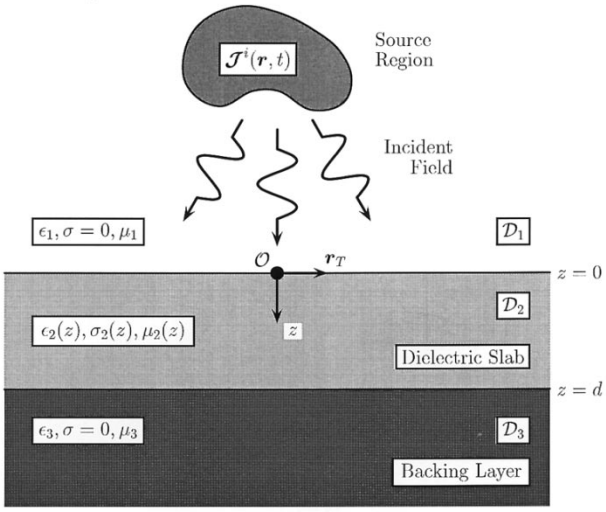

Fig. 1. Pulsed electric current above an inhomogeneous slab embedded between two homogeneous lossless half-spaces.

where $\mathbf{k}_T = k_x\mathbf{u}_x + k_y\mathbf{u}_y$ and $\mathbf{r}_T = x\mathbf{u}_x + y\mathbf{u}_y$ are vectors in the transverse plane. This transformation reduces the gradient operator in (2) to $i\mathbf{k}_T + \mathbf{u}_z\partial_z$ and the time differentiation to a scalar multiplication by $-i\omega$. We decompose the electromagnetic fields into their transverse and longitudinal parts, according to

$$\hat{\mathbf{E}}(\mathbf{k}_T,z,\omega) = \hat{\mathbf{E}}_T(\mathbf{k}_T,z,\omega) + \hat{E}_z(\mathbf{k}_T,z,\omega)\mathbf{u}_z \tag{4}$$

and we break up Maxwell's equations in the same manner. Next, the transverse field components are expressed in components parallel and orthogonal to the direction $\mathbf{k}_T/k_T$, according to

$$\hat{\mathbf{E}}_T = -i\frac{\mathbf{k}_T}{k_T}V^e + i\left(\mathbf{u}_z \times \frac{\mathbf{k}_T}{k_T}\right)V^h \tag{5a}$$

$$\hat{\mathbf{H}}_T = -i\left(\mathbf{u}_z \times \frac{\mathbf{k}_T}{k_T}\right)I^e - i\frac{\mathbf{k}_T}{k_T}I^h. \tag{5b}$$

In (5), the amplitudes $V^{e,h}(\mathbf{k}_T,z,\omega)$ and $I^{e,h}(\mathbf{k}_T,z,\omega)$ have, apart from a normalizing constant, the proper dimension of a frequency-domain current and voltage along a transmission line. Substituting (5) in the longitudinal part of Maxwell's equations leads to the identification

$$\tilde{\varepsilon}\hat{E}_z = \left(-k_T I^e + \hat{J}_z^e\right)\Big/ i\omega \tag{6a}$$

$$\mu\hat{H}_z = -k_T V^h/i\omega \tag{6b}$$

where we have introduced the usual frequency-domain permittivity

$$\tilde{\varepsilon}(z,\omega) = \varepsilon(z) - \sigma(z)/i\omega. \tag{7}$$

Equation (6) relates I^e and V^h to the longitudinal components of the electric and magnetic flux densities.

The expressions in (5) and (6) are substituted in the transverse parts of Maxwell's equations and, again, the components parallel and orthogonal to $\mathbf{k}_T/k_T$ are separated. This leads to

the desired transmission-line equations. For I^e and V^e, we arrive at

$$\partial_z I^e = i\omega\tilde{\varepsilon}V^e - \left(\frac{i\mathbf{k}_T}{k_T}\cdot\hat{\mathbf{J}}_T^i\right) \tag{8a}$$

$$\partial_z V^e = \frac{-i\gamma^2}{\omega\tilde{\varepsilon}}I^e + \frac{ik_T}{\omega\tilde{\varepsilon}}\hat{J}_z^i \tag{8b}$$

where $\gamma = \sqrt{(k_T)^2 - \omega^2\tilde{\varepsilon}(z)\mu(z)}$, with $\mathrm{Re}(\gamma) \geq 0$, and $\mathrm{Im}(\gamma) \leq 0$ when $\mathrm{Re}(\gamma) = 0$. This will be our choice of branch cut in all the square roots appearing in the rest of the paper. For I^h and V^h, the transmission-line equations read

$$\partial_z I^h = \frac{-i\gamma^2}{\omega\mu}V^h + \left(\mathbf{u}_z \times \frac{i\mathbf{k}_T}{k_T}\right)\cdot\hat{\mathbf{J}}_T^i \tag{9a}$$

$$\partial_z V^h = i\omega\mu I^h. \tag{9b}$$

From (8) and (9), we observe that the Fourier-transformed version of Maxwell's equations indeed has two independent solutions. The first one is determined by I^e and V^e. From (6) it follows that for this type of solution, only the electric field has a longitudinal component. Therefore, these solutions are indicated as E or TM modes [22]. The second solution is determined by I^h and V^h. For these solutions, only the magnetic field has a longitudinal component. Therefore, they are indicated as H or TE modes. Finally, (8) and (9) illustrate that the longitudinal component of $\hat{\mathbf{J}}^i$ only generates E modes. The term "modes" refers to the interpretation of a plane-stratified medium as an inhomogeneous waveguide with an infinite cross section. In this interpretation, propagation and attenuation take place in the z-direction, while the transverse eigenfunction is proportional to $\exp(i\mathbf{k}_T\cdot\mathbf{r}_T)$.

B. Second-Order Differential Equation

For a general type of continuous stratification, the systems of (8) and (9) must be solved numerically. In the literature, several techniques are described for solving such equations. We mention for example direct numerical integration ([23, sec. 2.4.2]) and wave splitting [24]. For reasons of efficiency, we prefer a generalization of the approach proposed in [10]. The first step is to reduce both (8) and (9) to a single second-order differential equation of the form

$$\alpha(z)\partial_z\left(\frac{1}{\alpha(z)}\partial_z\right)U(z) - \gamma^2(z)U(z) = F(z) \tag{10}$$

where only the dependence on z has been indicated explicitly. In (10), $\alpha(z)$ is a constitutive parameter, $U(z)$ is the unknown function, and $F(z)$ is the forcing function. In both cases, we choose the quantity that corresponds to a longitudinal flux density as the fundamental unknown.

When the impressed current density is a *vertical dipole*, applying the Fourier transformations (3a) and (3b) results in

$$\hat{J}_z^i(\mathbf{k}_T, z, \omega) = -i\omega S(\omega)\delta(z - z_0). \tag{11}$$

From (8), we then have

$$\alpha = \tilde{\varepsilon}, \quad U = I^e, \quad F = i\omega k_T S(\omega)\delta(z - z_0). \tag{12}$$

For a *horizontal dipole*, transforming the current density specified in (1) results in

$$\hat{\mathbf{J}}_T^i(\mathbf{k}_T, z, \omega) = -i\omega S(\omega)\delta(z - z_0)\mathbf{u}_x. \tag{13}$$

Substituting this result in (8) and (9) now gives

$$E\text{-modes:} \quad \alpha = \tilde{\varepsilon}, \quad U = I^e$$
$$F = -\frac{\omega k_x}{k_T}S(\omega) \times \left[\delta'(z - z_0) - \frac{\tilde{\varepsilon}'(z_0)}{\tilde{\varepsilon}(z_0)}\delta(z - z_0)\right] \tag{14a}$$

$$H\text{-modes:} \quad \alpha = \mu, \quad U = V^h$$
$$F = \frac{-i\omega^2\mu k_y}{k_T}S(\omega)\delta(z - z_0) \tag{14b}$$

where $\delta'(\cdot)$ is the derivative of the delta function. Since we have $z_0 < 0$ the factor of $\tilde{\varepsilon}'(z_0)$ in (14a) vanishes and the contribution proportional to $\delta(z - z_0)$ may be discarded. For the horizontal dipole, the differential equation (10) must be solved twice for each combination of $\mathbf{k}_T$ and ω. Once the fundamental unknowns I^e and V^h are known, it is straightforward to obtain V^e and I^h from (8a) and (9b).

III. Longitudinal Behavior

The first step toward solving the problem formulated in Section II is solving the differential equation (10) for the forcing functions given in (12) and (14) for a set of parameters $\{\mathbf{k}_T, \omega\}$ that allows the evaluation of the integrals in the inverse transformations of the ones given in (3a) and (3b). In this section, we address several aspects of this solution.

A. The Half-Spaces

In $\mathcal{D}_1$ the dielectric medium is homogeneous and lossless. The coefficients in (10) assume the constant values $\tilde{\varepsilon}(z) = \varepsilon_1, \mu(z) = \mu_1$, and the attenuation coefficient is $\gamma(z) = \gamma_1 = \sqrt{(k_T)^2 - \omega^2\varepsilon_1\mu_1}$. For the forcing functions specified above, we can therefore find a closed-form solution of this differential equation. For the vertical dipole, we have

$$U(z) = \frac{-i\omega k_T}{2\gamma_1}S(\omega)\{\exp(-\gamma_1|z - z_0|) + R^e\exp[\gamma_1(z + z_0)]\} \tag{15}$$

where R^e is an unknown reflection coefficient. This reflection coefficient is defined as the amplitude of the reflected wave that would be caused by the unit-amplitude incident wave $U^i(z) = \exp(-\gamma_1 z)$, when $\alpha(z) = \tilde{\varepsilon}_2(z)$ in the domain $\mathcal{D}_2$. For the horizontal dipole, we have

$$E\text{-modes:} \quad U(z) = -\frac{\omega k_x}{2k_T}S(\omega)\{\mathrm{sgn}(z - z_0) \times \exp(-\gamma_1|z - z_0|) + R^e\exp[\gamma_1(z + z_0)]\} \tag{16a}$$

$$H\text{-modes:} \quad U(z) = \frac{i\omega^2\mu_1 k_y}{2k_T\gamma_1}S(\omega)\{\exp(-\gamma_1|z - z_0|) + R^h\exp[\gamma_1(z + z_0)]\} \tag{16b}$$

where R^h is the amplitude of the reflected wave generated by $U^i(z)$ when $\alpha(z) = \mu_2(z)$ in $\mathcal{D}_2$.

Since the differential equation (10) is linear, this means that we may restrict ourselves, in the evaluation of the longitudinal behavior, to determining the response to a unit-amplitude plane wave for one or both of the possible choices of $\alpha(z)$. The multiplicative factors occurring in (5) and (6) and in (15) and (16) can then be included in the evaluation of the spectral integrals. Therefore, we consider the normalized solution $\breve{U}(z)$ of (10) which, in the homogeneous half-spaces, behaves as

$$\breve{U}(z) = \exp(-\gamma_1 z) + [\breve{U}(0) - 1]\exp(\gamma_1 z) \quad \text{for } z_0 < z < 0, \tag{17a}$$

$$\breve{U}(z) = \breve{U}(d)\exp[-\gamma_3(z-d)] \quad \text{for } d < z < \infty \tag{17b}$$

where $\gamma_3 = \sqrt{k_T^2 - \omega^2\varepsilon_3\mu_3}$, and where $\breve{U}(0) - 1 = R^{e,h}$. Obviously, the direct field for $z < z_0$ must also be adapted. However, for the homogeneous upper half-space considered in this paper, this field is available in closed form and should not be computed by spectral techniques.

B. Numerical Solution

To obtain $\breve{U}(z)$ for $0 \le z \le d$, we need to solve (10). To this aim we derive an equivalent contrast-source integral equation. For numerical convenience, we restrict ourselves to the case where $\varepsilon_2(z)$, $\sigma_2(z)$ and $\mu_2(z)$ are continuous functions of z in $0 < z < d$. Again, the analysis can directly be generalized to profiles with a finite number of discontinuities [5]. To arrive at the desired integral equation, we first define a spectral Green's function for an infinite, homogeneous, lossless reference configuration with permittivity $\bar{\varepsilon}$ and permeability $\bar{\mu}$. This function satisfies the differential equation

$$\left[\partial_z^2 + \omega^2\bar{\varepsilon}\bar{\mu} - k_T^2\right] G(z, z'; k_T, \omega) = -\delta(z - z') \tag{18}$$

and the radiation conditions as $|z| \to \infty$ and is known in closed form

$$G(z, z'; k_T, \omega) = \frac{1}{2\bar{\gamma}}\exp(-\bar{\gamma}|z - z'|) \tag{19}$$

where $\bar{\gamma} = \sqrt{k_T^2 - \omega^2\bar{\varepsilon}\bar{\mu}}$. Next, we apply the one-dimensional version of Green's second identity for $\breve{U}(z)$ and $G(z, z')$ over the interval $0 < z < d$. This results in

$$\int_0^d \left[G\partial_z^2\breve{U} - \breve{U}\partial_z^2 G\right] dz = G\partial_z\breve{U} - \breve{U}\partial_z G\big|_{z=0}^{z=d}. \tag{20}$$

In (20), we substitute (10) and (18) to eliminate the second derivatives in the integrand on the left-hand side. In the evaluation of the end-point contributions in the right-hand side, we use the known behavior of $\breve{U}(z)$ in $\mathcal{D}_1$ and $\mathcal{D}_3$ as specified in (17). From the continuity of $\breve{U}(z)$ and $\alpha^{-1}(z)\partial_z\breve{U}(z)$ (implied by (10)) we then derive the boundary conditions

$$\lim_{z\downarrow 0}\partial_z\breve{U}(z) = \gamma_1\frac{\alpha_2(0)}{\alpha_1}[\breve{U}(0) - 2],$$

$$\lim_{z\uparrow d}\partial_z\breve{U}(z) = -\gamma_3\frac{\alpha_2(d)}{\alpha_3}\breve{U}(d). \tag{21}$$

With these conditions and (19), the right-hand side of (20) is reduced to the sum of a known excitation term and two terms proportional to $\breve{U}(0)$ and $\breve{U}(d)$. By equating the results obtained for both sides of (20) we then arrive at the desired integral equation

$$\begin{aligned}\breve{U}(z) = {} & \frac{\alpha_2(0)\gamma_1}{\alpha_1\bar{\gamma}}\exp(-\bar{\gamma}z) - \frac{1}{2\bar{\gamma}}\int_0^d \exp(-\bar{\gamma}|z - z'|) \\ & \times \frac{\alpha_2'(z')}{\alpha_2(z')}\partial_{z'}\breve{U}(z')\,dz' + \frac{\omega^2}{2\bar{\gamma}}\int_0^d \exp(-\bar{\gamma}|z - z'|) \\ & \times [\tilde{\varepsilon}_2(z', \omega)\mu_2(z') - \bar{\varepsilon}\bar{\mu}]\breve{U}(z')\,dz' \\ & + \frac{\alpha_1\bar{\gamma} - \alpha_2(0)\gamma_1}{2\alpha_1\bar{\gamma}}\breve{U}(0)\exp(-\bar{\gamma}z) \\ & + \frac{\alpha_3\bar{\gamma} - \alpha_2(d)\gamma_3}{2\alpha_3\bar{\gamma}}\breve{U}(d)\exp(-\bar{\gamma}[d - z])\end{aligned} \tag{22}$$

where z and z' have been interchanged, where $\alpha'(z')$ denotes the derivative of $\alpha(z')$, and where it has been assumed that $0 \le z \le d$. Equation (22) expresses the unknown field as a superposition of plane waves traveling in the homogeneous reference configuration. The first term on the right-hand side is a direct wave that corresponds to the incident plane wave in (17a). The next two terms are integrals that represent the influence of the induced sources inside the slab. The last two impedance-like terms account for the reflections at the interfaces with the exterior half-spaces. In principle, the choice of the reference medium is arbitrary. From a computational point of view, it seems sensible to choose $\bar{\varepsilon}$ and $\bar{\mu}$ such that a (locally) propagating wave in the actual configuration is always represented in terms of propagating waves in the reference medium.

To solve (22) numerically, we introduce a uniform spatial grid $z_m = m\Delta z$, with $m = 0, 1, \ldots, M$ and $\Delta z = d/M$. The value of M is chosen independently of the values of the spectral parameters k_T and ω. We enforce (22) at the grid points, and approximate the integrals over z' by a repeated trapezoidal rule. For the evaluation of the space derivative in the factor $\partial z'\breve{U}(z')$, we use central differences for the interior points and the conditions (21) at the slab's boundaries. We then end up with a discretized equation of the form

$$\begin{aligned}\breve{U}_m = {} & AZ^{-m} + \sum_{m'=1}^{M-1} Z^{-|m-m'|}B_{m'}[\breve{U}_{m'+1} - \breve{U}_{m'-1}] \\ & + \sum_{m'=0}^{M} Z^{-|m-m'|}C_{m'}\breve{U}_{m'}\end{aligned} \tag{23}$$

where $Z = \exp(\bar{\gamma}\Delta z)$ and where the subscripts refer to the corresponding points in discretized space.

The system of (23) can be inverted by a fully recursive solution procedure, which is a generalization of the one proposed in [10]. The procedure consists of three principal steps. First, the rows with $m = 1, \ldots, M$ are reduced to a convenient three-diagonal form by carrying out three simple row operations. In the second step, the rows with $m = 1, \ldots, M$ are used to successively remove the leftmost element of the row with $m = 0$, which remains unchanged in the first step. Moving the reduced first row to position M then results in a matrix equation with a system matrix whose only nonvanishing elements are on the diagonal and the first two superdiagonals. In the third step, this system is solved by back substitution. Details will be published elsewhere.

The solution procedure described above combines the advantages that the accuracy of the solution obtained is of $\mathcal{O}(M^{-2})$ and the computation time is of $\mathcal{O}(M)$ als $M \to \infty$. Further, the boundary conditions at $z = 0$ and $z = d$ as given in (21) are incorporated in closed form, which leads to an improved accurary compared with a discretization of (8) or (9) and these conditions with the aid of finite differences. A possible problem is that, for large values of k_T, $\breve{U}(z)$ shows a strong exponential decay for increasing z. Now the reduction of row(0) in step 2 outlined above results in the reciprocal of the transmission coefficient of the slab. Therefore, the numerical implementation of this step may suffer from overflow problems. These problems can be avoided by monitoring the magnitude of the factor $\exp(\gamma_1 z_0)$, which appears in all the amplitudes derived from (12) and (14).

C. Asymptotic Behavior

For large values of one or both of the parameters ω and k_T, an asymptotic solution of the differential equation (10) can be derived. By scaling the spatial wave vector $\mathbf{k}_T$ according to

$$\mathbf{k}_T = \frac{\omega}{c_0}\boldsymbol{\nu}_T \tag{24}$$

where c_0 is the speed of light in free-space, we can handle both cases simultaneously. When $\alpha = \tilde{\varepsilon}$, i.e., for E modes, we have the complication that this coefficient is frequencydependent. Therefore, we derive the solution for that case. The solution for $\alpha = \mu$, i.e., for H-modes, is then obtained from analogy.

As argued above, we only determine the response to a unit-amplitude plane wave. With the definition (7) and the scaling specified above, the differential equation (10), can then be written as

$$\left[\partial_z^2 - \frac{\varepsilon'(z) + i\sigma'(z)/\omega}{\varepsilon(z) + i\sigma(z)/\omega}\partial_z - \frac{\omega^2}{c_0^2}u^2(z) + i\omega\mu(z)\sigma(z)\right]\breve{U}(z) = 0 \tag{25}$$

where the prime denotes differentiation, where $\breve{U}(z) = I^e(\mathbf{k}_T, z)$, and where $u(z) = \sqrt{(\nu_T)^2 - \varepsilon_r(z)\mu_r(z)}$. $u(z)$ is almost the scaled scaled counterpart of $\gamma(z)$, but the term with $\sigma(z)$ in (25) is treated separately. Equation (25) is not yet in a suitable form for deriving a WKB approximation of its solution. However, such a form is obtained immediately by expanding the logarithmic derivative of $\varepsilon(z) + i\sigma(z)/\omega$ in a geometrical series in powers of ω^{-1}.

The analysis is based on ideas presented in [23, secs. 2.3.3, 2.5.3]. From [25], we know that, in any region where the coefficients of (25) are continuous with derivatives that are discontinuous at no more than a finite number of points, there exist two linearly independent solutions $\breve{U}^{\pm}(z)$ whose first-order WKB approximations are given by

$$\breve{U}_a^{\pm}(z; z_1) = \sqrt{\frac{\varepsilon_r(z)u(z_1)}{\varepsilon_r(z_1)u(z)}} \times \exp\left\{\mp\int_{z_1}^{z}\left[\frac{\omega}{c_0}u(z') + \frac{Z_0\mu_r(z')\sigma(z')}{2iu(z')}\right]dz'\right\} \tag{26}$$

where Z_0 is the free-space impedance. In (26) the superscript $\pm$ indicates the direction of propagation, and the wave originates from the point $z = z_1$. With this result, we can formally write

$$\breve{U}(z) = \begin{cases} \exp(-\gamma_1 z) + R^e\exp(\gamma_1 z) & \text{in } \mathcal{D}_1 \\ P^e\breve{U}_a^{+}(z;0) + Q^e\breve{U}_a^{-}(z;d) & \text{in } \mathcal{D}_2, \\ T^e\exp[-\gamma_3(z-d)] & \text{in } \mathcal{D}_3 \end{cases} \tag{27}$$

where only the coefficients R^e, P^e, Q^e and T^e are still unknown. These coefficients are found by enforcing the continuity of $\breve{U}(z)$ and $\tilde{\varepsilon}^{-1}(z)\partial_z\breve{U}(z)$ at $z = 0$ and $z = d$. The derivatives of $\breve{U}_a^{\pm}(z; z_1)$ are found in first approximation by utilizing the fact that differentiation of a WKB approximation of a given accuracy yields the derivative of the solution to the same accuracy [25].

For the reflection coefficient R^e, for example, we then obtain the following first-order approximation:

$$R_a^e = R_{1,2}^{e,a} + \frac{T_{1,2}^{e,a}\breve{U}_a^{+}(d;0)R_{2,3}^{e,a}\breve{U}_a^{-}(0;d)T_{2,1}^{e,a}}{1 - R_{2,1}^{e,a}\breve{U}_a^{+}(d;0)R_{2,3}^{e,a}\breve{U}_a^{-}(0;d)} \tag{28}$$

where the asymptotic reflection and transmission coefficients at the slab's interfaces are given by

$$R_{1,2}^{e,a} = \frac{\varepsilon_2(0)u_1 - \varepsilon_1 u_2(0)}{\varepsilon_2(0)u_1 + \varepsilon_1 u_2(0)}, \quad R_{2,1}^{e,a} = \frac{\varepsilon_1 u_2(0) - \varepsilon_2(0)u_1}{\varepsilon_1 u_2(0) + \varepsilon_2(0)u_1}$$
$$R_{2,3}^{e,a} = \frac{\varepsilon_3 u_2(d) - \varepsilon_2(d)u_3}{\varepsilon_3 u_2(d) + \varepsilon_2(d)u_3}, \quad T_{1,2}^{e,a} = \frac{2\varepsilon_2(0)u_1}{\varepsilon_2(0)u_1 + \varepsilon_1 u_2(0)}$$
$$T_{2,1}^{e,a} = \frac{2\varepsilon_1 u_2(0)}{\varepsilon_1 u_2(0) + \varepsilon_2(0)u_1} \tag{29}$$

where $u_j = \sqrt{(\nu_T)^2 - \varepsilon_{jr}\mu_{jr}}$ for $j = 1, 3$. Similar expressions are found for P^e, Q^e and T^e.

Finally, we must repeat the analysis for the H modes. However, only the logarithmic derivative in (25) changes for this type of modes. In deriving (26), we have only used the first-order approximation of this term. The same approximation was used in the application of the boundary conditions. Therefore, we can immediately find the asymptotic solution for the Hmodes by replacing ε by μ in the term with the square root in (26) and in the asymptotic reflection and transmission coefficients defined in (29). The factor $\mu_r(z')$ in the exponent in (26) need not be replaced, since the term with $\sigma(z)$ in (25) remains as is.

D. Singularities in the Complex ν_T-Plane

As a function of complex ν_T, the spectral constituent $U(z)$ representing $I^e(\omega\boldsymbol{\nu}_T/c_0, z, \omega)$ or $V^h(\omega\boldsymbol{\nu}_T/c_0, z, \omega)$ has two types of singularities. In the first place, there are two branch cuts in the upper half of the complex ν_T-plane with branch points at $\nu_T = n_1 = \sqrt{\varepsilon_{1r}\mu_{1r}}$ and $\nu_T = n_3 = \sqrt{\varepsilon_{3r}\mu_{3r}}$. These branch cuts are associated with the choice of the "physical" root in the attenuation coefficients $\gamma_1 = \omega u_1/c_0$ and $\gamma_3 = \omega u_3/c_0$ in the boundary conditions (21). In the transform domain, the problem is completely defined by these boundary conditions and the second-order differential equation (10) in the interval $0 \le z \le d$. This differential equation only contains a term $\gamma^2 = \omega^2 u_2^2(z)/c_0^2$; therefore no extra branch cuts are introduced for the interior of $\mathcal{D}_2$.

In the second place, we need to consider the occurrence of so-called guided-wave poles. As shown in Appendix A, for $\sigma_2(z) = 0$ such poles only occur in the interval

$$\max\{n_1, n_3\} < \nu_T < \max\{n_2(z)\,|\,0 < z < d\} \tag{30}$$

where $n_2(z) = \sqrt{\varepsilon_{2r}(z)\mu_{2r}(z)}$ is the local refractive index in $\mathcal{D}_2$, provided that this interval exists. Each pole corresponds to a homogeneous solution of Maxwell's equations that propagates in the transverse direction. The location of the poles, and their number, depends on ω. For $\sigma_2(z) > 0$, the poles occur in the first quadrant of the complex ν_T-plane, and approach the same interval as $\omega \to \infty$. Now, the integration contour may be considered as running just below the real ν_T-axis. Therefore, numerical problems will occur in the solution of the integral equation (22) for ν_T in that interval since this equation does not have a unique solution for values of ω that correspond to guided-wave poles.

IV. Transformation to the Space–Time Domain

Once $I^{e,h}$ and $V^{e,h}$ have been computed, the longitudinal components of the fields can be calculated from (6) and subsequently the transverse components from (5). The final step in the procedure is to carry out the inverse Fourier transformations corresponding to (3a) and (3b). As mentioned at the end of Subsection III.A, we need to multiply the unit-amplitude solution discussed in Sections III-B and C by the multiplicative factors occurring in (15) and (16). To keep the paper legible, we restrict the discussion to the reflected field in $\mathcal{D}_1$ since this is the field that would be measured in applications in inverse scattering and antenna design. However, the ideas presented in this chapter are also directly applicable to the total fields in $\mathcal{D}_2$ and $\mathcal{D}_3$. For the incident field in $\mathcal{D}_1$, difficulties are encountered near the source point $\mathbf{r} = z_0\mathbf{u}_z$. As mentioned above, this field is available in closed form and need not be computed by spectral techniques.

A. Spectral Field Components

For the vertical dipole, only the E-modes are excited. The transform-domain reflected-field components are given by

$$\hat{E}_z^r(\mathbf{k}_T, z, \omega) = \frac{k_T^2}{2\gamma_1\varepsilon_1} S(\omega) R^e(k_T, \omega) \exp[\gamma_1(z + z_0)] \tag{31a}$$

$$\hat{\mathbf{H}}_T^r(\mathbf{k}_T, z, \omega) = \frac{-\omega(\mathbf{u}_z \times \mathbf{k}_T)}{2\gamma_1} S(\omega) R^e(k_T, \omega) \times \exp[\gamma_1(z + z_0)] \tag{31b}$$

$$\hat{\mathbf{E}}_T^r(\mathbf{k}_T, z, \omega) = \frac{i\mathbf{k}_T}{2\varepsilon_1} S(\omega) R^e(k_T, \omega) \exp[\gamma_1(z + z_0)]. \tag{31c}$$

For the horizontal dipole, adding the contributions of the E- and H-modes results in

$$\hat{E}_z^r(\mathbf{k}_T, z, \omega) = \frac{-ik_x}{2\varepsilon_1} S(\omega) R^e(k_T, \omega) \exp[\gamma_1(z + z_0)] \tag{32a}$$

$$\hat{H}_z^r(\mathbf{k}_T, z, \omega) = \frac{-k_y\omega}{2\gamma_1} S(\omega) R^h(k_T, \omega) \exp[\gamma_1(z + z_0)] \tag{32b}$$

$$\hat{\mathbf{H}}_T^r(\mathbf{k}_T, z, \omega) = \frac{i\omega}{2k_T^2} S(\omega) [(\mathbf{u}_z \times \mathbf{k}_T) k_x R^e(k_T, \omega) + \mathbf{k}_T k_y R^h(k_T, \omega)] \exp[\gamma_1(z + z_0)], \tag{32c}$$

$$\hat{\mathbf{E}}_T^r(\mathbf{k}_T, z, \omega) = \frac{S(\omega)}{2k_T^2} \left[\frac{\mathbf{k}_T k_x \gamma_1}{\varepsilon_1} R^e(k_T, \omega) - \omega^2 \frac{(\mathbf{u}_z \times \mathbf{k}_T) k_y}{\gamma_1} R^h(k_T, \omega) \right] \times \exp[\gamma_1(z + z_0)]. \tag{32d}$$

In (31) and (32) $R^{e,h}$ are the reflection coefficients introduced in (15) and (16).

The obvious approach to determine, from (31) and (32), the corresponding space-time fields is to evaluate each of the inversion integrals corresponding to (3a) and (3b) directly with the aid of fast Fourier transformations. An example for acoustic waves is described in [26]. However, this requires considerable computational effort, even in the case of a piecewise-homogeneous or two-media configuration. To speed up the calculations, we cast the Fourier inversion into a special form that was also used in the half-space configurations considered in [3] and [4]. To illustrate the procedure, without excessively extending the paper, we consider two representative field components in (31) and (32), viz. $\hat{E}_z(\mathbf{k}_T, z, \omega)$ for the vertical dipole and $\hat{E}_x(\mathbf{k}_T, z, \omega)$ for the horizontal one.

B. Weyl Representations

Let us start with $\hat{E}_z^r(\mathbf{k}_T, z, \omega)$ for the vertical dipole. First, we restrict the temporal Fourier inversion to nonnegative frequencies by expressing the time-domain signal as

$$\mathcal{E}_z^r(\mathbf{r}, t) = \mathrm{Re}\{\mathcal{E}_z^{r+}(\mathbf{r}, t)\} \tag{33}$$

with

$$\mathcal{E}_z^{r+}(\mathbf{r}, t) = \frac{1}{\pi} \int_0^\infty d\omega \exp(-i\omega t) E_z^r(\mathbf{r}, \omega). \tag{34}$$

Here, $\mathcal{E}_z^{r+}(\mathbf{r}, t)$ represents the dual analytic signal corresponding to $\mathcal{E}_z^r(\mathbf{r}, t)$. This signal is an analytic function in the lower half of the complex t-plane $\mathrm{Im}(t) \leq 0$, and its real part approaches $\mathcal{E}_z^r(\mathbf{r}, t)$ when $\mathrm{Im}(t) \uparrow 0$.

The restriction to $\omega \geq 0$ allows us to use the normalized spatial transform vector ν_T introduced in (24). Further, since $\hat{E}_z(\mathbf{k}_T, z, \omega)$ only depends on k_T, we also change over to the normalized cylindrical coordinates $\{\nu_T, \varphi_\nu\}$. The spatial Fourier inversion corresponding to (3b) then assumes the form

$$E_z^r(\mathbf{r}, \omega) = \frac{\omega^2}{4\pi^2 c_0^2} \int_0^\infty \nu_T \, d\nu_T \int_{-\pi}^{\pi} d\varphi_\nu \hat{E}_z^r(\nu_T, \varphi_\nu, z, \omega) \times \exp\left(i \frac{\omega \nu_T}{c_0} r_T \cos(\varphi_\nu - \varphi) \right) \tag{35}$$

where $\{r_T, \varphi, z\}$ are cylindrical coordinates in actual space.

Combining (31a), (34), and (35) and reversing the order of the temporal and spatial Fourier inversions then leads to the so-called frequency-domain Weyl representation for the reflected field

$$\mathcal{E}_z^{r+}(\mathbf{r}, t) = \frac{-iZ_0}{8\pi^2 c_0^2} \int_{-\pi}^{\pi} d\varphi'_\nu \int_0^\infty d\nu_T \frac{\nu_T^3}{u_1(\nu_T)\varepsilon_{1r}} \times \left\{ \frac{1}{\pi} \int_0^\infty d\omega (-i\omega)^3 S(\omega) R^e(\nu_T, \omega) \times \exp[-i\omega(t - \tau(\nu_T, \varphi'_\nu, z))] \right\} \tag{36}$$

where the complex time delay is given by

$$\tau(\nu_T,\varphi'_\nu,z)=\frac{\nu_T}{c_0}r_T\cos(\varphi'_\nu)-\frac{iu_1(\nu_T)}{c_0}(z+z_0) \qquad (37)$$

and where the definition for $u_1(\nu_T)$ was given after (29). Because the cosine in (35) is periodical, the variable in the angular integration has been changed to $\varphi'_\nu=\varphi_\nu-\varphi$, and $E_z^r(\mathbf{r},\omega)$ does not depend on φ.

Repeating the same procedure for the dual analytic signal corresponding to $\mathcal{E}_x^r(\mathbf{r},t)$ for the case of the horizontal dipole, we obtain

$$\begin{aligned}\mathcal{E}_x^{r+}(\mathbf{r},t)=&\frac{-iZ_0}{8\pi^2c_0^2}\int_{-\pi}^{\pi}d\varphi'_\nu\int_0^\infty\nu_T\,d\nu_T\\&\times\left\{\frac{1}{\pi}\int_0^\infty d\omega(-i\omega)^3S(\omega)\right.\\&\times\left[\cos^2(\varphi'_\nu+\varphi)\frac{u_1(\nu_T)}{\varepsilon_{1r}}R^e(\nu_T,\omega)\right.\\&\left.\left.+\sin^2(\varphi'_\nu+\varphi)\frac{\mu_{1r}}{u_1(\nu_T)}R^h(\nu_T,\omega)\right]\right.\\&\left.\times\exp[-i\omega(t-\tau(\nu_T,\varphi'_\nu,z))]\right\}. \qquad (38)\end{aligned}$$

Apart from constant amplitudes and a factor of $(-i\omega)^3$, the terms in braces in (36) and (38) are of the same form as the right-hand side in (34) and the complex time argument $t-\tau(\nu_T,\varphi'_\nu,z)$ cannot have a positive imaginary part. Therefore, these terms can be identified as time derivatives of dual analytic signals. This observation is used to derive a suitable combination of Gaussian quadrature rules for the evaluation of the integral over ν_T. Compared with an evaluation by fast Fourier transform (FFT) operations, this has the advantage that the number of values of ν_T for which the numerical computation outlined in Section III-B must be performed is reduced considerably.

C. Contour Deformation and Quadrature

To obtain the quadrature rule, we must first analyze the situation in the complex ν_T-plane. The analysis is carried out in two steps. We first consider the dual analytic signals

$$\mathcal{R}^{p+}(\nu_T,t)=\frac{1}{\pi}\int_0^\infty d\omega\,S(\omega)R^p(\nu_T,\omega)\exp(-i\omega t) \qquad p=e,h \quad (39)$$

for a fixed t with $\mathrm{Im}(t)\le 0$. Subsequently, we will then consider the consequences of taking a ν_T-dependent time delay as given in (37).

For a fixed t, the singularities in the integrand in (39) originate from the reflection coefficients $R^{e,h}(\nu_T,\omega)$. For a given ω, these singularities were analyzed in Section III-D. As remarked there, we have two types.

1) In the first place, there are two *branch cuts* in the complex wavenumber plane. After the normalization of $\mathbf{k}_T$ carried out above, these singularities show up as the branch cuts in the normalized attenuation coefficients u_1 and u_3. These branch cuts are present for all frequencies and, hence, will also be observed in $\mathcal{R}^{e,h+}(\nu_T,t)$.
2) In the second place, there are *guided-wave poles*. As discussed in Section III-C, for $\sigma_2(z)=0$ these poles are located on the interval specified in (30), provided that this interval exists. The integration over ω in (39) reduces the influence of the poles. According to the generalization of the Mittag–Leffler theorem for a function with isolated poles to the case where the function has one or more branch cuts, $\mathcal{R}^{e,h+}(\nu_T,t)$ only has an extra jump discontinuity along this interval. For $\sigma_2(z)>0$, each point in the subinterval is a condensation point for guided-wave poles at different values of ω. Therefore, the behavior along the real ν_T-axis will be similar to that in the lossless case.

The definition of $u_j=\sqrt{\nu_T^2-n_j^2}$ was chosen such that the integration contour may be regarded as running along the real ν_T axis in the fourth quadrant of the complex ν_T-plane. Therefore, the situation in the complex ν_T-plane may be envisaged as indicated in Fig. 2, where it is assumed that $n_3>n_1$ since in practical configurations the upper medium is usually free-space.

To ensure that the spectral integral equation (22) has a solution, we deform the contour into the lower half of the complex ν_T-plane as indicated in Fig. 3. In doing so, we need to choose ℓ_1 large enough to avoid a possible ill-posedness of the discretized integral equation (23), and possible difficulties in the numerical integration along the interval between $n_3-i\ell_1$ and $n_3-i\ell_1+\ell_2$. To investigate to what extent this is allowed, we write the frequency-domain Weyl representation (36) in terms of the dual analytic signal introduced in (39). This leads to the so-called time-domain Weyl representation for the z-component of the electric field in the case of the vertical dipole

$$\begin{aligned}\mathcal{E}_z^{r+}(\mathbf{r},t)=&\frac{-iZ_0}{8\pi^2c_0^2}\int_{-\pi}^{\pi}d\varphi'_\nu\int_0^\infty d\nu_T\,\frac{\nu_T^3}{u_1(\nu_T)\varepsilon_{1r}}\\&\times\partial_t^3\mathcal{R}^{e+}(\nu_T,t-\tau(\nu_T,\varphi'_\nu,z)). \qquad (40)\end{aligned}$$

For the x-component of the electric field generated by a horizontal dipole we find

$$\begin{aligned}\mathcal{E}_x^{r+}(\mathbf{r},t)=&\frac{-iZ_0}{8\pi^2c_0^2}\int_{-\pi}^{\pi}d\varphi'_\nu\int_0^\infty\nu_T\,d\nu_T\\&\times\left[\cos^2(\varphi'_\nu+\varphi)\frac{u_1(\nu_T)}{\varepsilon_{1r}}\right.\\&\times\partial_t^3\mathcal{R}^{e+}(\nu_T,t-\tau(\nu_T,\varphi'_\nu,z))\\&+\sin^2(\varphi'_\nu+\varphi)\frac{\mu_{1r}}{u_1(\nu_T)}\\&\left.\times\partial_t^3\mathcal{R}^{h+}(\nu_T,t-\tau(\nu_T,\varphi'_\nu,z))\right]. \qquad (41)\end{aligned}$$

Since all singularities in the integrand in the right half of the complex ν_T-plane are located on or above the real ν_T-axis, no extra contributions are encountered in this deformation.

However, the definition (39) of $\mathcal{R}^{e,h+}(\nu_T,t)$ may only be applied for $\mathrm{Im}(t)\le 0$. In principle, $\mathcal{R}^{e,h+}(\nu_T,t)$ can be continued analytically into the half plane $\mathrm{Im}(t)>0$, but we need (39) in the numerical computations. With the aid of the asymptotic expansions in Section III-C and a suitable definition of $\mathcal{S}(t)$ in (1), it follows that the imaginary part of the time arguments in (40)

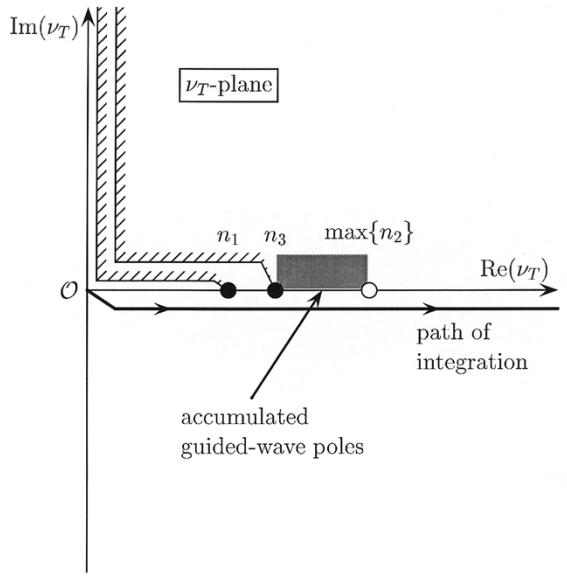

Fig. 2. Path of integration in the complex ν_T plane.

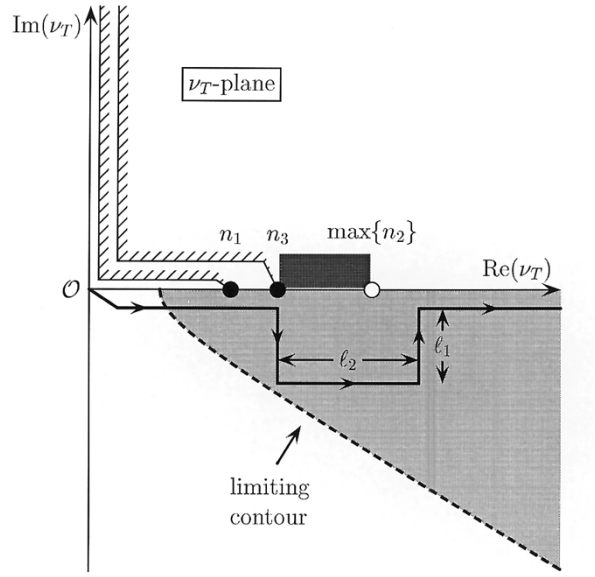

Fig. 3. Contour deformation in the complex ν_T plane.

and (41) must be nonpositive for all z and φ'_ν. This implies that the limiting contour is given by

$$-\nu_T r_T + i u_1 z_0 = n_1 \ell \tag{42}$$

where ℓ is a real-valued length parameter. Solution of this equation leads to one of the well-known representations of the Cagniard contour for a point on the interface at $z = 0$ with respect to the source point at $\mathbf{r} = z_0 \mathbf{u}_z$

$$\nu_T = n_1 \frac{r_T \ell \pm |z_0| \sqrt{r^2 - \ell^2}}{r^2}. \tag{43}$$

This contour intersects the real ν_T-axis at $\nu_T = n_1 r_T / r$, and the angle of the asymptote with that axis is given by $\tan\alpha = |z_0|/r_T$. The limiting contour is given by z_0 and the maximum value of r_T for which we want to compute $\mathcal{E}^r_{x,z}(\mathbf{r}, t)$. A typical example is shown in Fig. 3.

An advantage of (40) and (41) is that these representations allow us to devise a composite Gaussian quadrature rule which is valid for all t and for all $\mathbf{r}$ with r_T smaller than a given maximum offset. We restrict ourselves to the case where the contour deformation is necessary, i.e., where $\max\{n_2\} > \max\{n_1, n_3\}$. The simpler case when the contour may be chosen along the real ν_T axis is handled in an analogous manner. Up to $\nu_T = n_3 + \ell_2$, the contour is broken up into straight segments ending at $\nu_T = 0$, n_1, $(n_1 + n_3)/2$, n_3, $n_3 - i\ell_1$, $n_3 - i\ell_1 + \ell_2$ and $n_3 + \ell_2$. In all intervals, a single Gauss–Legendre rule is used and stretching is employed to convert the integrand to a suitable form.

The semi-infinite subinterval $n_3 + \ell_2 < \nu_T < \infty$ requires special attention. To choose the proper quadrature rule, we use the property that the asymptotic approximation of Section III-C is also valid for a fixed ν_T and $\omega \to \infty$. With the definition (39), we then have

$$\begin{aligned}\mathcal{R}^{e+}_a(\nu_T, t) = T^{e,a}_{1,2} R^{e,a}_{2,3} T^{e,a}_{2,1} \sum_{n=0}^{\infty} \Bigg\{ & \left(R^{e,a}_{1,2} R^{e,a}_{2,3}\right)^n \\ & \times \exp\left(-nZ_0 \int_0^d \frac{\mu_r(z')\sigma(z')}{iu(z')}\, dz'\right) \\ & \times \mathcal{S}^+\left(t - (2n+2)\int_0^d \frac{iu(z')}{c_0}\, dz'\right)\Bigg\}\end{aligned} \tag{44}$$

and a similar result for $\mathcal{R}^{h+}_a(\nu_T, t)$. The expression in (44) can be simplified further by realizing that $u(z) = \nu_T + \mathcal{O}(\nu_T^{-1})$ as $\nu_T \to \infty$.

On the final part of the interval, we now use the substitution $\nu_T = n_1 \cosh(\xi)$ to account for the factor $u_1 = n_1 \sinh(\xi)$ in the denominator. From the large-argument behavior of analytic signals described in Appendix B, it then follows that the integrands of (40) and (41) decay as $\exp(-2\xi)$, independently of the values of $\mathbf{r}$ and t. This allows the application of a Gauss–Laguerre quadrature rule. Depending on the value of z_0, which controls the attenuation of the integrand for $t - (\nu_T/c_0) r_T \cos(\varphi'_\nu) \approx 0$, this behavior sets in for larger values of ν_T. To handle the initial part of the interval, a repeated low-order Gauss–Legendre rule is used that is capable of handling the local oscillations that occur when the time argument in (40) or (41) is close to zero.

Once the quadrature rule is derived, we proceed exactly as described in [3] and [4]. First, the integral over ν_T in (36) is replaced by the discretized form derived for (40). Next, the integral over φ'_ν is evaluated in closed form with the aid of [21, eq. 9.1.21]

$$\begin{aligned}\int_0^\pi \cos(n\varphi'_\nu) \exp\left(\frac{i\omega\nu_T}{c_0} r_T \cos(\varphi'_\nu)\right) d\varphi'_\nu \\ = \pi i^n J_n\left(\frac{\omega\nu_T}{c_0} r_T\right), \quad n = 0, 1, 2, \ldots, \infty.\end{aligned} \tag{45}$$

Finally, the integral over ω is truncated, discretized with the aid of a repeated trapezoidal rule, and cast into the form of an FFT operation.

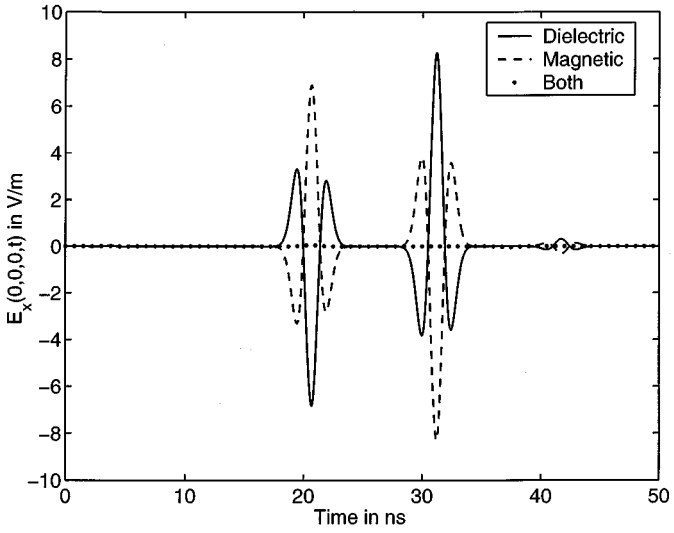

Fig. 4. x-component of the reflected electric field at the point $(0, 0, 0)$ versus time. Configuration parameters: $d = 1$ m and $z_0 = -5$ m. Solid line: dielectric with $\varepsilon_{2r}(z) = 2+z, \mu_{2r}(z) = 1$. Broken line: magnetic slab with $\varepsilon_{2r}(z) = 1$, $\mu_{2r}(z) = 2 + z$. Dotted line: $\varepsilon_{2r}(z) = \mu_{2r}(z) = 2 + z$.

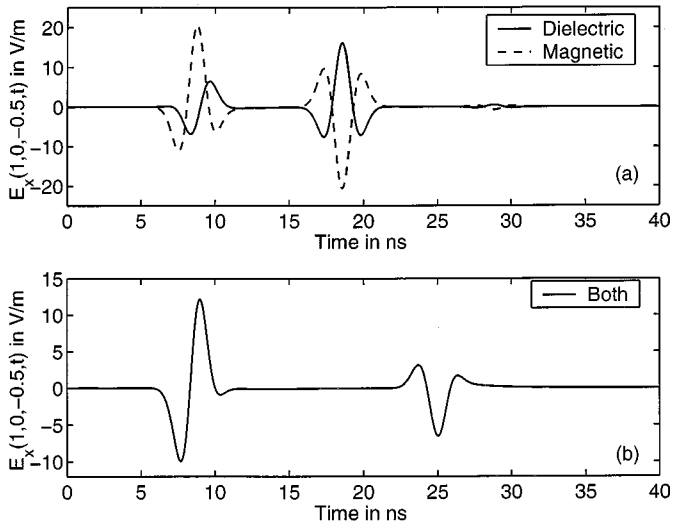

Fig. 5. x-component of the reflected electric field versus time at the point $(1, 0, -0.5)$ m. Configuration parameters: $d = 1$ m and $z_0 = -0.5$ m. (a) Solid line: dielectric with $\varepsilon_{2r}(z) = 2 + z$, $\mu_{2r}(z) = 1$. Broken line: magnetic slab with $\varepsilon_{2r}(z) = 1$, $\mu_{2r}(z) = 2 + z$. (b) Solid line: $\varepsilon_{2r}(z) = \mu_{2r}(z) = 2 + z$.

V. Results

Numerical results were obtained for a variety of configurations. We restrict ourselves here to present a few examples that briefly illustrate the performance of the method. All of them correspond to the case of a horizontal dipole located above an inhomogenous slab in free-space. The driving current density of the dipole is given by (1) with $\mathcal{S}(t) = \exp[-(gt - 4)^2]$ and $g = 10^9 s^{-1}$. As an observation variable we have chosen the time signature of the x-component of the reflected electric field $\mathcal{E}_x^r(x, y, z, t)$ at some specific points in the upper medium. The examples were chosen such that the time-domain results will also appeal to the reader's physical intuition.

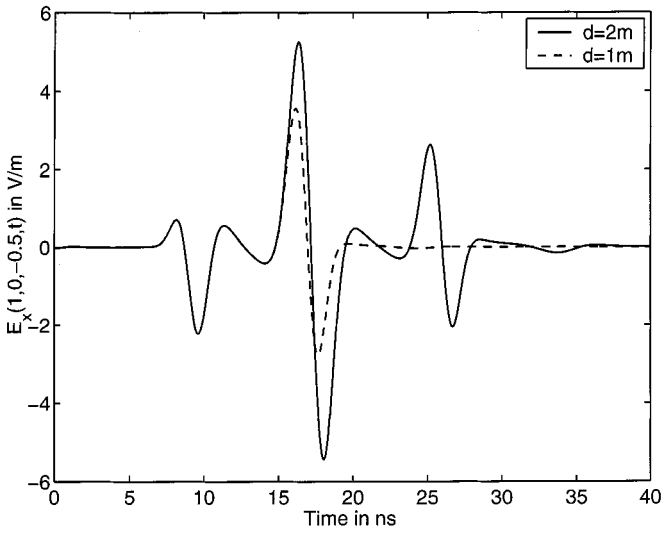

Fig. 6. x-component of the reflected electric field at the observation point $(1, 0, -0.5)$ m versus time. Dielectric slab with $\varepsilon_{2r}(z) = 1 + 2\sin^2(\pi z)$. $z_0 = -0.5$ m. Solid line: slab width $d = 2$ m. Broken line: slab width $d = 1$ m.

First, we analyze the behavior of the configuration described above when the inhomogeneous slab, with width $d = 1$ m, is one of the following: 1) a dielectric material with $\varepsilon_{2r}(z) = 2 + z$, $\mu_{2r}(z) = 1$; 2) a magnetic material with $\mu_{2r}(z) = 2 + z$, $\varepsilon_{2r}(z) = 1$; and 3) both, i.e., $\varepsilon_{2r}(z) = \mu_{2r}(z) = 2 + z$. The dipole is located at a distance above the slab of either $|z_0| = 5$ m or $|z_0| = 0.5$ m. Fig. 4 shows $\mathcal{E}_x^r(x, y, z, t)$ versus time at the observation point $(0, 0, 0)$, which is located at the interface between medium 1 and 2 just below the dipole, when $|z_0| = 5$ m. From Fig. 4 it can be observed that the response for the dielectric contrast is approximately the same, but with opposite sign, as that for magnetic contrast and that when both contrasts are present, the reflected field is approximately zero. This is the behavior that should be expected when the dipole is relatively far from the slab and a plane wave at normal incidence can be assumed to be impinging on it. Fig. 5 shows the solution obtained for the same configuration when $|z_0| = 0.5$ m, the observation point is $(1, 0, -0.5)$ m and all other parameters remain unchanged. Now the responses for the dielectric and magnetic contrasts no longer have the same amplitude. Furthermore, when both profiles are present, the reflected field in the upper medium is not negligible. Observe also how in the latter case the propagation inside the slab is slower than in the dielectric or magnetic cases and the response plotted in Fig. 5(b) progressively delays with respect to that shown in Fig. 5(a).

As a last example we consider two inhomogeneous slabs with the same relative permittivity profile $\varepsilon_{2r}(z) = 1 + 2\sin^2(\pi z)$ but with different widths; the first one with $d = 1$ m and the second one with $d = 2$ m. In both cases the relative permeability is $\mu_{2r}(z) = 1$. The horizontal dipole is located at a distance $|z_0| = 0.5$ m above either of the slabs and the observation point is $(1, 0, -0.5)$ m. The x-component of the time-domain reflected fields is shown in Fig. 6. It is observed that the two signals are identical until the arrival of the fields reflected at $z = 1$ m.

VI. Conclusion

In this paper, we have formulated a new strategy for determining transient fields generated by a pulsed, vertical, or horizontal electric dipole over a plane-stratified, lossy dielectric slab between two homogenenous half-spaces. The general idea was to consider all spatial approximations in the time domain. This has led to a fixed discretization which, in the actual computations, is used in the frequency domain. The underlying mathematics is rather complicated, but the numerical implementation as such is quite simple. Once the quadrature rule has been selected, the only difference with a more conventional implementation is that the number of spectral field components that must be computed is reduced considerably. In addition, we can accept a relative error in these components that increases for larger frequencies and nevertheless remain in control of the accuracy in the time domain. The results obtained satisfy our physical intuition.

The scheme presented in this paper is able to efficiently compute time-domain Green's functions in piecewise continuously layered media, provided that certain restrictions on the pulse shape of the impressed current or incident field may be imposed. Further, dispersion effects can be handled without significantly increasing the computational effort. This makes our approach extremely suitable for computing background effects in antenna design or inverse scattering, e.g., for applications in ground penetrating radar. Applications of modeling straight and circular wire antennas over homogeneous and layered half-spaces have already been completed successfully.

Appendix I
Location of Guided Wave Poles in the ν_T-Plane

As remarked in Section III-D, the reflection coefficients $R^{e,h}$ may have poles in the complex k_T-plane due to the occurrence of guided-wave modes. Such modes correspond to homogeneous solutions of the second-order differential equation (10), with $|U(z)| \to 0$ as $|z| \to \infty$. With the choice of $\gamma(z)$ as specified in (8), this decay can be achieved by choosing k_T away from the branch cuts, and by selecting the proper closed-form solutions in $\mathcal{D}_1$ and $\mathcal{D}_3$. Matching these solutions via the boundary conditions to the solution of the differential equation (10) in $\mathcal{D}_2$ then results in a characteristic equation for the propagation coefficient k_T. For a general inhomogeneous configuration both (10) and the characteristic equation must be solved numerically.

In this appendix, we derive bounds on the values of k_T for which such guided-wave modes may occur. To this end, we follow an idea that was originally proposed in [27] and later described in more detail in [28]. Starting point of the analysis is the differential equation (10) in which we substitute the definition of $\gamma(z)$ given in (8) and the scaling $k_T = \omega\nu_T/c_0$ introduced in (24). Further, we factor out the relative permeability and permittivity. We thus obtain

$$\partial_z\left(\frac{1}{\alpha_r(z)}\partial_z\right)U(z) - \frac{\omega^2}{c_0^2}\left[\nu_T^2 - \tilde{\varepsilon}_r(z,\omega)\mu_r(z)\right]\frac{1}{\alpha_r(z)}U(z) = 0. \quad \text{(A.1)}$$

Now, we multiply all terms in (A.1) by $U^*(z)$, where the asterisk denotes complex conjugation, and we integrate over $-\infty < z < \infty$. This is allowed, because $U(z)$ is an exponentially decreasing function as $|z| \to \infty$. Using integration by parts, we then obtain the identity

$$\nu_T^2\int_{-\infty}^{\infty}\frac{1}{\alpha_r(z)}|U(z)|^2\,dz = \int_{-\infty}^{\infty}\frac{\tilde{\varepsilon}_r(z,\omega)\mu_r(z)}{\alpha_r(z)}|U(z)|^2\,dz - \frac{c_0^2}{\omega^2}\int_{-\infty}^{\infty}\frac{1}{\alpha_r(z)}|\partial_z U(z)|^2\,dz. \quad \text{(A.2)}$$

The bounds for the possible values of ν_T now follow by taking the real and imaginary parts.

A. H Modes

Let us first consider the case of H polarization, for which we observe from (14b) that $\alpha_r(z) = \mu_r(z)$. Since $\varepsilon_r(z)$, $\sigma(z)$, $\mu_r(z)$ and ω are all real-valued and nonnegative, (A.2) can be decomposed into

$$\mathrm{Re}\left(\nu_T^2\right)\int_{-\infty}^{\infty}\frac{1}{\mu_r(z)}|U(z)|^2\,dz = \int_{-\infty}^{\infty}\varepsilon_r(z)|U(z)|^2\,dz + \frac{c_0^2}{\omega^2}\int_{-\infty}^{\infty}\frac{1}{\mu_r(z)}|\partial_z U(z)|^2\,dz \quad \text{(A.3)}$$

$$\mathrm{Im}\left(\nu_T^2\right)\int_{-\infty}^{\infty}\frac{1}{\mu_r(z)}|U(z)|^2\,dz = \int_{-\infty}^{\infty}\frac{\sigma(z)}{\omega\varepsilon_0}|U(z)|^2\,dz. \quad \text{(A.4)}$$

From these relations, we immediately derive the inequalities

$$0 < \mathrm{Re}\left(\nu_T^2\right) \le \max\{\varepsilon_r(z)\mu_r(z)\} \quad \text{(A.5)}$$

$$\frac{1}{\omega\varepsilon_0}\min\{\sigma(z)\mu_r(z)\} \le \mathrm{Im}\left(\nu_T^2\right) \le \frac{1}{\omega\varepsilon_0}\max\{\sigma(z)\mu_r(z)\} \quad \text{(A.6)}$$

where the minima and maxima are taken over the interval $-\infty < z < \infty$.

A detailed analysis of the consequences of (A.5) and (A.6) can be found in [27]. In the present context, the following observations are sufficient. For a *lossless* slab, guided wave poles are only observed in a finite interval on the real ν_T-axis. This interval is constrained still further by the requirement that ν_T may not be chosen on the branch cuts. Taking this condition into account leads to

$$\max\{n_1, n_3\} < \nu_T \le \max\{n_2(z)\,|\,0 < z < d\} \quad \text{(A.7)}$$

where we have introduced the index of refraction $n_2(z) = \sqrt{\varepsilon_{2r}(z)\mu_{2r}(z)}$. For a *lossy* slab with $\sigma_2(z) > 0$, the guided wave poles are located in the first quadrant of the complex ν_T-plane, which is in agreement with the physical condition that the guided-wave modes must attenuate in the

direction of propagation. As $\omega \to \infty$, these poles approach the interval on the real ν_T-axis specified in (A.7).

B. E Modes

For the case of E polarization $\alpha_r(z) = \tilde{\varepsilon}_r(z,\omega) = \varepsilon_r(z) + i\sigma(z)/(\omega\varepsilon_0)$. For $\sigma(z) = 0$, the analysis is completely analogous to the one given above for the H modes. Therefore, we may consider the case where $\sigma(z) > 0$ for some values of z. Taking the real and imaginary parts of (A.2) now results in

$$\begin{aligned}\operatorname{Re}\left(\nu_T^2\right) &\int_{-\infty}^{\infty} \varepsilon_r(z) \left|\frac{U(z)}{\tilde{\varepsilon}_r(z,\omega)}\right|^2 dz \\ &= \int_{-\infty}^{\infty} \mu_r(z)|U(z)|^2\, dz - \frac{c_0^2}{\omega^2}\int_{-\infty}^{\infty} \varepsilon_r(z)\left|\frac{\partial_z U(z)}{\tilde{\varepsilon}_r(z,\omega)}\right|^2 dz \\ &\quad - \operatorname{Im}\left(\nu_T^2\right)\int_{-\infty}^{\infty}\frac{\sigma(z)}{\omega\varepsilon_0}\left|\frac{U(z)}{\tilde{\varepsilon}_r(z,\omega)}\right|^2 dz \qquad \text{(A.8)}\end{aligned}$$

$$\begin{aligned}\operatorname{Im}\left(\nu_T^2\right) &\int_{-\infty}^{\infty} \varepsilon_r(z) \left|\frac{U(z)}{\tilde{\varepsilon}_r(z,\omega)}\right|^2 dz \\ &= \operatorname{Re}\left(\nu_T^2\right)\int_{-\infty}^{\infty}\frac{\sigma(z)}{\omega\varepsilon_0}\left|\frac{U(z)}{\tilde{\varepsilon}_r(z,\omega)}\right|^2 dz \\ &\quad + \frac{c_0^2}{\omega^2}\int_{-\infty}^{\infty}\frac{\sigma(z)}{\omega\varepsilon_0}\left|\frac{\partial_z U(z)}{\tilde{\varepsilon}_r(z,\omega)}\right|^2 dz. \qquad \text{(A.9)}\end{aligned}$$

We restrict the analysis of these identities to the case $\operatorname{Re}(\nu_T^2) > 0$, which covers the two quarter planes located nearest to the real ν_T-axis. Then, from (A.9) we deduce that

$$\operatorname{Im}\left(\nu_T^2\right) \geq \operatorname{Re}\left(\nu_T^2\right)\min\left\{\frac{\sigma(z)}{\omega\varepsilon(z)}\right\} \qquad \text{(A.10)}$$

and

$$\begin{aligned}\operatorname{Im}\left(\nu_T^2\right) \leq \max\left\{\frac{\sigma(z)}{\omega\varepsilon(z)}\right\}&\left[\operatorname{Re}\left(\nu_T^2\right)\right. \\ &\left. + \frac{c_0^2}{\omega^2}\frac{\int_{-\infty}^{\infty}\varepsilon_r(z)\left|\frac{\partial_z U(z)}{\tilde{\varepsilon}_r(z,\omega)}\right|^2 dz}{\int_{-\infty}^{\infty}\varepsilon_r(z)\left|\frac{U(z)}{\tilde{\varepsilon}_r(z,\omega)}\right|^2 dz}\right]. \qquad \text{(A.11)}\end{aligned}$$

Equation (A.10) implies that $\operatorname{Im}(\nu_T^2) \geq 0$, which together with (A.8) leads us to

$$\operatorname{Re}\left(\nu_T^2\right) \leq \max\left\{\varepsilon_r(z)\mu_r(z) + \frac{\mu_r(z)}{\varepsilon_r(z)}\left(\frac{\sigma(z)}{\omega\varepsilon_0}\right)^2\right\} \qquad \text{(A.12)}$$

where the definition of $\tilde{\varepsilon}_r(z,\omega)$ has been substituted.

Equations (A.10)–(A.12), are the counterparts of (A.5) and (A.6). Although they are more complicated, they lead to similar conclusions for the location of the guided wave poles in the complex ν_T-plane. In particular, from the asymptotic expressions derived in Section III.C it can be seen that the quotient of the two integrals in (A.11) is of order ω^2/c_0^2 as $\omega \to \infty$ and, therefore, these poles still approach the real ν_T-interval specified in (A.7). Finally, it should be remarked that the results found in this appendix are simpler than the ones found in [28]. This is an advantage of considering the problem in the ν_T-domain rather than in the k_T-domain.

APPENDIX II
PROPERTIES OF DUAL ANALYTIC SIGNALS

The analysis in this paper relies strongly on the theory of dual analytic signals. The concept of analytic signal originates from Gabor [29], and has found extensive application in communication theory. Rather complete bibliographies and a summary of their properties can be found in [30] and [31]. In this appendix, we restrict ourselves to those properties that are needed to handle the spectral representation for the configuration at hand.

For a time signal $\mathcal{S}(t)$ with spectrum $S(\omega)$, we define the dual analytic signal as

$$\mathcal{S}^+(t) = \frac{1}{\pi}\int_0^{\infty} S(\omega)\exp(-i\omega t)\, d\omega. \qquad \text{(B.13)}$$

$\mathcal{S}^+(t)$ is an analytic function of t in the lower half-plane $\operatorname{Im}(t) < 0$ and its derivatives are the dual analytic signals corresponding to the derivatives of $\mathcal{S}(t)$. It is readily verified that

$$\mathcal{S}^+(t) = \frac{1}{\pi i}\int_{-\infty}^{\infty}\frac{\mathcal{S}(t')}{t-t'}\, dt. \qquad \text{(B.14)}$$

When t approaches the real t-axis from below, we have

$$\begin{aligned}\mathcal{S}^+(t-i0) &= \mathcal{S}(t) - i\mathcal{S}_H(t), \\ \mathcal{S}_H(t) &= \frac{1}{\pi}\mathcal{P}\int_{-\infty}^{\infty}\frac{S(t')}{t-t'}\, dt' \qquad \text{(B.15)}\end{aligned}$$

where $\mathcal{P}$ denotes the principal value, and where $\mathcal{S}_H(t)$ is the Hilbert transform of $\mathcal{S}(t)$.

For our analysis, we also need the asymptotic behavior as $|t| \to \infty$. When the time signal $\mathcal{S}(t')$ vanishes for $|t'| > T$, the factor of $1/(t-t')$ can be expanded in a power series in t'/t. This leads to

$$\mathcal{S}^+(t) = \frac{1}{\pi i}\sum_{n=0}^{\infty}\frac{A_n}{t^{n+1}}, \quad \text{with } A_n = \int_{-\infty}^{\infty}(t')^n\mathcal{S}(t')\, dt' \qquad \text{(B.16)}$$

being the moments of the signal $\mathcal{S}(t)$. When this signal has infinite duration, not all the moments $\{A_n\}$ may exist. However, we can still use a partial sum of the geometrical series to derive a similar result.

In both cases, it is clear that the first nonvanishing moment of $\mathcal{S}(t)$ determines the rate of decay of $\mathcal{S}^+(t)$ as $|t| \to \infty$. For example, for the third derivative that occurs in (40) and (41), the dual analytic signal behaves as

$$\partial_t^3\,\mathcal{S}^+(t) \approx \frac{6iA_0}{\pi t^4} \quad \text{as } |t| \to \infty \text{ in } \operatorname{Im}(t) \leq 0. \qquad \text{(B.17)}$$

ACKNOWLEDGMENT

Many of the ideas described in this paper originate from a collaboration of the first author with Prof. E. F. Kuester, University of Colorado at Boulder. Further, both authors would like to thank Profs. H. Blok and A. T. de Hoop, Delft University of Technology, The Netherlands, and Dr. E. S. A. M. Lepelaars,

TNO Physics and Electronics Laboratory, The Hague, for many stimulating discussions.

REFERENCES

[1] J. R. Wait, *Electromagnetic Waves in Stratified Media*. New York: IEEE Press, 1996. 2nd ed..

[2] J. R. Wait and D. A. Hill, "Fields of a horizontal loop of arbitrary shape buried in a two-layer earth," *Radio Sci.*, vol. 15, pp. 903–912, 1980.

[3] A. Rubio Bretones and A. G. Tijhuis, "Transient excitation of a straight thin wire segment over an interface between two dielectric half spaces," *Radio Sci.*, vol. 30, pp. 1723–1738, 1995.

[4] ——, "Transient excitation of two coupled wires over an interface between two dielectric half spaces," *Radio Sci.*, vol. 32, pp. 25–41, 1997.

[5] E. S. A. M. Lepelaars, "Transient electromagnetic excitation of biological media by circular loop antennas," Ph.D. dissertation, Eindhoven Univ. Technology, The Netherlands, 1997.

[6] A. J. Devaney and G. C. Sherman, "Plane-wave representations for scalar wave fields," *SIAM Rev.*, vol. 15, pp. 765–786, 1973.

[7] R. W. P. King and S. S. Sandler, "The electromagnetic field of a vertical electric dipole in the presence of a three-layered region," *Radio Sci.*, vol. 29, pp. 97–113, 1994.

[8] S. L. Dvorak, "Application of the fast Fourier transform to the computation of the Sommerfeld integral for a vertical electric dipole above a half-space," *IEEE Trans. Antennas Propagat.*, vol. 40, pp. 798–805, July 1992.

[9] S. L. Dvorak and M. M. Mechaik, "Application of the contour transformation method to a vertical dipole over earth," *Radio Sci.*, vol. 28, pp. 309–317, 1993.

[10] A. G. Tijhuis, R. Wiemans, and E. F. Kuester, "A hybrid method for solving time-domain integral equations in transient scattering," *J. Electromagn. Waves Applicat.*, vol. 3, pp. 485–511, 1989.

[11] A. G. Tijhuis and Z. Q. Peng, "Marching-on-in-frequency method for solving integral equations in transient electromagnetic scattering," *Proc. Inst. Elect. Eng.*, pt. H, pp. 347–355, 1991.

[12] A. T. de Hoop, "A modification of Cagniard's method for solving seismic pulse problems," *Appl. Sci. Res.*, vol. B8, pp. 349–356, 1960.

[13] A. T. de Hoop and H. J. Frankena, "Radiation of pulses generated by a vertical electric dipole above a plane nonconducting earth," *Appl. Sci. Res.*, vol. B8, pp. 370–377, 1960.

[14] H. J. Frankena, "Transient phenomena associated with Sommerfeld's horizontal dipole problem," *Appl. Sci. Res.*, vol. B8, pp. 357–368, 1960.

[15] C. H. Chapman, "Generalized ray theory for an inhomogeneous medium," *Geophys. J. R. Astrolog. Soc.*, vol. 36, pp. 673–704, 1974.

[16] ——, "Exact and approximate generalized ray theory in vertically inhomogeneous media," *Geophys. J. R. Astrolog. Soc.*, vol. 46, pp. 201–233, 1976.

[17] E. Heyman and L. B. Felsen, "Non-dispersive closed form approximations for transient propagation and scattering of ray fields," *Wave Motion*, vol. 7, pp. 335–358, 1985.

[18] ——, "Weakly dispersive spectral theory of transients—Part I: Formulation and interpretation," *IEEE Trans. Antennas Propagat.*, vol. AP-35, pp. 80–86, Jan. 1987.

[19] ——, "Weakly dispersive spectral theory of transients, part 2: Evaluation of the spectral integral," *IEEE Trans. Antennas Propagat.*, vol. AP-35, pp. 574–580, May 1987.

[20] E. Heyman, "Weakly dispersive spectral theory of transients, part 3: Applications," *IEEE Trans. Antennas Propagat.*, vol. AP-35, pp. 1258–1266, Nov. 1987.

[21] M. A. Abramowitz and I. A. Stegun, *Handbook of Mathematical Functions*. New York: Dover, 1965.

[22] L. B. Felsen and N. Marcuvitz, *Radiation and Scattering of Waves*, 2nd ed. New York: IEEE Press, 1994, sec. 2.2.

[23] A. G. Tijhuis, *Electromagnetic Inverse Profiling; Theory and Numerical Implementation*. Utrecht, The Netherlands: VNU Sci. Press, 1987.

[24] G. Kristensson, "Transient electromagnetic wave propagation in waveguides," *J. Electromagn. Waves Applicat.*, vol. 9, pp. 645–671, 1995.

[25] A. Erdélyi, *Asymptotic Expansions*. New York: Dover, 1956, ch. 4.

[26] J. T. Fokkema, P. M. van den Berg, and M. Vissinga, "On the computation of Radon transforms of sesimic data," *J. Seism. Explorat.*, vol. 1, pp. 93–105, 1992.

[27] H. M. de Ruiter, "Limits on the propagation constants of planar optical waveguide modes," *Appl. Opt.*, vol. 20, pp. 731–732, 1981.

[28] W. C. Chew, *Waves and Fields in Inhomogeneous Media*, 2nd ed. New York: IEEE Press, 1995, sec. 2.7.2.

[29] D. Gabor, "Theory of communication—Part I," *J. Inst. Elect. Eng.*, vol. 93, pp. 429–441, 1946.

[30] M. Born and E. Wolf, *Principles of Optics*, 5th ed. Oxford, U.K.: Pergamon, 1975, pp. 494–499.

[31] J. L. Brown, "Analytic signals and product theorems for Hilbert transforms," *IEEE Trans. Circuits Syst.*, vol. 21, pp. 790–792, 1974.

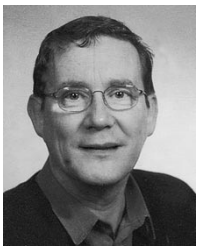

Anton G. Tijhuis (M'88) was born in Oosterhout N.B., The Netherlands. He received the M.Sc. degree in theoretical physics from Utrecht University, The Netherlands, in 1976, and the Ph.D. degree (*cum laude*) from Delft University of Technology, The Netherlands, in 1987.

From 1976 to 1993, he was employed at the Laboratory of Electromagnetic Research, Faculty of Electrical Engineering, Delft University of Technology, initially as an Assistant Professor and, since 1986, as an Associate Professor. From 1991 to 1992, he was a member of the Executive Board of the Faculty of Electrical Engineering as Vice Chairman for Research. Since 1993, he has been a Full Professor of Electromagnetics at the Faculty of Electrical Engineering, Eindhoven University of Technology. In addition, he is Scientific Advisor to the TNO Physics and Electronics Laboratory, Gravenhage, The Netherlands. He has been a Visiting Scientist at the University of Colorado at Boulder, McDonnell Research Laboratories, Saint Louis, MO, Tel-Aviv University, Israel, and on several occasions at the Universidad de Granada, Spain. His current research interests are the theory of electromagnetic fields, in particular, efficient modeling techniques and their application in electromagnetic detection and synthesis problems.

Amelia Rubio Bretones (SM'99) was born in Granada, Spain. She received the Ph.D. degree in physics (*cum laude*) from the University of Granada, Spain, in 1988.

Since 1985 she has been with the Department of Electromagnetism at the University of Granada, where she is currently an Associate Professor. She was a Visiting Scientist at Delft and Eindhoven Universities of Technology (both in The Netherlands) and at the Pennsylvania State University, University Park. Her research interests are mainly in the field of numerical techniques for applied electromagnetics with emphasis on time-domain techniques such as finite-difference time-domain, the application of method of moments in the time domain for antenna and scattering problems, and hybrid techniques.